Engineering Failure Analysis 138 (2022) 106328

Contents lists available at ScienceDirect

Engineering Failure Analysis

journal homepage: www.elsevier.com/locate/engfailanal

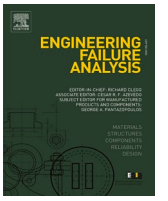

Fatigue failure transition evaluation of load carrying cruciform welded joints by effective notch energy model

Guangtao Zhou [a], Jingzhen Kuang [a], Wei Song [b,*], Guian Qian [c], Filippo Berto [d]

[a] College of Mechanical Engineering and Automation, Huaqiao University, Xiamen 361021, China
[b] School of Mechanical & Electrical Engineering, Xuzhou University of Technology, Xuzhou 221018, China
[c] LNM, Institute of Mechanics, Chinese Academy of Sciences, Beijing 100190, China
[d] Department of Mechanical and Industrial Engineering, Norwegian University of Science and Technology (NTNU), Richard Birkelands vei 2b, 7491 Trondheim, Norway

ARTICLE INFO

Keywords:
Load-carrying welded joint
Low and high cycle fatigue
Material heterogeneity
Failure transition
Effective notch energy

ABSTRACT

This paper investigates fatigue failure transition boundary of Load-carrying Cruciform Weld Joint (LCWJ) with different yield strength mismatch ratios and geometrical sizes of welded joints under cyclic loading conditions using a semi-empirical analytical method, which is based on the obtained fatigue test data and finite element analysis. To examine the fatigue failure mode transition relationship in CLWJs, different mismatch ratios and local geometries (plate thickness, weld size, and penetration ratio) were designed and fabricated to evaluate potential fatigue initiations (weld toe or weld root). The numerical simulations of cyclic responses at weld toe and weld root were conducted by material cyclic plastic properties from fatigue data of standard coupon specimens. A uniform effective notch energy indicator in the previous investigation was utilized to characterize the low and high cycle fatigue life by extending the SED method on the combination of generalized Neuber concept of Fictitious Notch Rounding (FNR). The related analytical formulations for potential failure points were used to predict the fatigue assessment indicator of LCWJ, considering the effects of plasticity and mechanical heterogeneity and geometry configurations. The effective notch energy relationship between the weld toe and weld root in LCWJ was determined by the established analytical solutions, verified by the fatigue data. The strategy is expected to provide some insights into assessing fatigue life for various types of weld joints for different potential failure locations.

1. Introduction

Marine structures active in coastal, offshore, and deep-sea are subjected to overlarge force, moment, or cyclic loading induced by the environment and structural service conditions. The Load-carrying Cruciform Weld Joint (LCWJ) was one of the essential joint types of the marine structures, which exists two potential fatigue failure points in this joint, Weld Toe (W.T.) and Weld Root (W.R.). These potential fatigue cracks impose some possible threats to the safety of serviced welded structures, although some post-welding treatments, such as HFMI, TIG dressing, grinding processing, could be conducted to enhance the fatigue life by decreasing the notch stress concentration or releasing part of tensile residual stress. On the other hand, the fatigue crack initiation point depends not only on the sizes of weld geometries and penetration length of fusion metal but also on the interaction effect between cyclic loadings and material

* Corresponding author.

https://doi.org/10.1016/j.engfailanal.2022.106328
Received 21 February 2022; Received in revised form 10 April 2022; Accepted 14 April 2022
Available online 2 May 2022

properties, especially for the LCF regime. Fatigue of welded joint was often assessed by the localized procedure considering the above various factors. However, the local approaches of welded joints in the LCF regime exhibit more complicated work during the computational processing of fatigue characteristic values. Therefore, calculating characteristic fatigue values based on the elasto-plastic mechanical theory is crucial for assessing the fatigue failure behavior of welded joints.

Determining fatigue crack initiation points and predicting fatigue life for welded joints or engineering structures depends on the geometric parameters, material properties, and cyclic loading conditions [1]. Compared with extensive HCF failure assessment of welded components [2-7], the geometric effect considering the material properties in the LCF regime needs to conduct more additional experimental and numerical analysis using fatigue damage and elasto-plastic mechanical theory. Japanese researchers [8] comprehensively evaluated the fatigue life and crack initiations of LCWJs incorporating the LCF and HCF failure. The size effect and low-temperature effect of non-loading carrying cruciform welded joints on LCF behaviors were investigated [9].

To quantify local plastic deformation near W.T. or W.R. locations, different fatigue indicators characterizing the crack driving forces based on stress, strain, or strain energy density were employed to calculate the magnitude evolution of the discontinuous geometric positions. According to the standard code, the effective notch stress ($\rho_{notch} = 1$ mm) is usually employed to compute the local stress as the fatigue indicator for HCF failure, avoiding the notch stress singularity. Moreover, the hot-spot stress method was also common in evaluating the fatigue failure behaviors, illustrating the stress-raising effect caused by the global geometrical discontinuity [10,11]. Additionally, the master S-N method based on Equivalent Traction Structural Stress (ETSS) by extracting the nodal forces and nodal moments is an alternative procedure to assess the fatigue behaviors of welded components [12]. It makes the fatigue assessment procedure convenient due to the mesh insensitivity [13]. The ETSS method was subsequently used for the fatigue assessment of various welded components, such as the marine and offshore structures [14], bridge structures [15,16], girth-welded pipes [17]. In order to determine the fatigue failure mode transition relationship between W.T. and W.R. locations quantitively, Xing et al. [18] carried out a series of fatigue tests of LCWJs considering the main and attachment plate thickness in the range from 8 mm to 22 mm. The fatigue data transferability among different titanium welded joint types was analyzed using the ETSS parameter [19]. Meanwhile, the axial and angular misalignment effects on the fatigue behavior of welded joints were also examined by an analytical model derived by ETSS [20,21].

However, the stress-based method is inaccurate to evaluate the LCF failure behavior due to the slight variations when the notch locations occur plasticity hardening under strain loading conditions. The effective notch strain is an alternative parameter to characterize the local plastic deformation. Kawin Saiprasertkit et al. [22] utilized the method to establish a related model for predicting fatigue indicator magnitudes in LCWJ by elasto-plastic analysis. The effective notch strain model was used to evaluate the fatigue initiation points and accommodate the local plastic deformation around the notches in LCWJ, considering the geometric sizes and material strength mismatch ratios. The related semi-experience analytical expressions of W.T. and W.R. were estimated to determine the fatigue crack initiations [23]. Recently, a modified effective notch strain approach was developed for the fatigue reliability assessment of JCWJs in LCF and HCF regimes, which considered the uncertainties of weld geometry, material properties, and the loading conditions [24].

On the other hand, the structural strain definition with a closed-form plasticity correction was introduced to illustrate the local fatigue characteristics in the LCF regime by Dong et al. [25]. Some fatigue tests data of welded components made by the high strength structural steel, aluminum alloy, and titanium alloys were reanalyzed by the equivalent structural strain parameter range under the LCF loadings. A unified master E-N curve was presented to estimate LCF and HCF fatigue life [26]. Another advantage of the structural strain range indicator is mesh-insensitive for potential applications in the future, which is effective for illustrating notch singularity due to the local notch concentrations. To extend the local approach in the LCF regime, an effective notch energy method was proposed to correct the local plastic deformation in welded joints. The energy-based approach is the comprehensive mechanical indicator, which incorporates the stress and strain components in the fatigue damage assessment.

For the HCF assessment, the fatigue strength of weld toe failure in LCWJ is FAT63, which is higher than that of weld root failure (FAT36). The fatigue strength discrepancy mainly depends on the relationship between the weld size and penetration length. The fatigue fracture mode in LCWJ can be transited from the W.T. to W.R. with the decreases of penetration or weld sizes. Thus, failure mode transition has a critical size boundary, which can judge the fatigue crack initiation point. It will effectively prevent W.R. cracking by modifying the weld size and penetration. For the LCF behavior of LCWJ, however, the critical size boundary depends on not only the weld geometries but also the material mismatch ratios between the base metal and weldment. The interaction relationship between weld sizes and material properties becomes more complicated for LCWJ.

This paper will focus on the fatigue crack initiation locations in LCWJs under HCF and LCF loadings by the effective notch energy approach. As shown in Section 2, the investigation starts with the introduction of fatigue experiments regarding the materials and welded joints under different loading conditions. In Section 3, the fatigue test results in the LCF and HCF regimes will be presented to illustrate the fatigue indicator variations. Furthermore, the effective notch energy-based method is exhibited by finite element analysis results and analytical solutions. The related analytical model based on the elasto-plastic mechanical analysis is utilized to predict the fatigue crack initiation points in LCWJ. Finally, the fatigue failure relationship between W.T. and W.R. is judged according to the analytical solutions.

2. Material properties and experimental details

10CrNi3MoV high strength steel as the base metal was selected to investigate the mechanical properties received in the quenched and tempered condition. Single Pulsed Gas Metal Arc Welding (SP-GMAW) processing was conducted to manufacture the butt welded joints with a V-groove with an evenmatched corresponding wire (wire diameter Φ 1.2 mm). Conversely, the Gas Metal Arc Welding

(GMAW) processing was performed for undermatched welded joints by the filler metal with a lower yield strength (wire diameter Φ 1.2 mm). The related chemical compositions of these materials were presented in the Table 1 [27]. Furthermore, the mechanical properties of these materials under monotonic and cyclic tension loading conditions were also investigated and presented in Ref. [27], which is presented in Fig. 1. As seen in Fig. 1, the cyclic stress–strain curve by Ramberg-Osgood (R-O) relationship equation for 10CrNi3MoV is lower than that of undermatched weldment, which means undermatched welded joints for the base metal. It should be noted that the mismatch ratio is defined according to the material cyclic yield strength from cyclic stress–strain curves.

Fig. 2(a) depicts the local geometries of the LCWJ specimen. It gives some related geometrical items, including notch radius ρ, weld length h, main plate thickness t, transverse plate thickness L, and penetration length p. According to the geometric relationship in LCWJ, the crack length (2a) at W.R. equals to t-p. The relationship between the fused weld size and the plate thickness is defined as the penetration ratio. Fig. 2(b) shows the schemes of LCWJs with different penetration ratios (0.7, 0.3, and 0). To fabricate line crack with different penetration ratios at weld root in LCWJ specimens, we first punch a small hole in the middle of the specimen using the electro-spark technique. Then, the weld root crack was made by the wire-electrode method to achieve the different penetration lengths. The actual LCWJs with a crack at weld root were also presented in Fig. 2(b). The related geometric configurations of LCWJ and fatigue tests were summarized in Ref. [28].

3. Experimental results

3.1. Crack initiation points and propagation locus

According to previous investigations about the fatigue failure behaviors of the LCWJ joints, the LCF and HCF test programs were both conducted to examine the load-carrying abilities for welded components under displacement-controlled and force-controlled loading conditions, respectively. The LCF tests of LCWJs were carried out utilizing the 250KN Instron servo-hydraulic machine under constant displacement-controlled amplitudes. The strain amplitudes of LCWJ samples cover from 0.2% to 0.6% under the strain ratio $R_\varepsilon = 0.1$. It should be noted that the calibrated 50 mm gauge length extensometer attached on the LCWJ specimens is employed to monitor the strain variations in the LCF tests. A low frequency range from 0.1 Hz to 3 Hz was utilized to carry out the LCF tests according to the applied loading levels. The LCF test was stopped as a maximum loading force loss 30% from the initial state. The HCF experimental procedure on LCWJ under load-controlled conditions is described in [28]. The higher frequency range of HCF for LCWJs lies from 10 to 20 Hz under the stress ratio $R = 0.1$.

Fig. 3 shows the fatigue crack initiation points and crack growth locus in LCWJ under cyclic strain loading conditions considering different material strengths and geometry configurations. Fig. 3(a)-(c) stands for the cases of undermatched welded joints, while Fig. 3 (d)-(f) depicts the failure cases of evenmatched welded joints. In Fig. 3(a), the weld root crack initiates and propagates to a specific position. Meanwhile, the crack at W.T. will initiate and grow to a certain length. Then, it propagates rapidly along the boundary between the HAZ and weldment due to the variation of load-carrying force lines. As demonstrated in Fig. 3(b), the crack initiates from W.R. and propagates towards W.T. in undermatched LCWJs with large penetration length ratios (p/t = 0.5 and 0.7). Furthermore, the fatigue crack propagation locus also occurs in the boundary between weldments and HAZ. As for the joints with an incomplete penetration ratio (M = 0), the fatigue crack can propagate through the undermatched weldments directly, which is depicted in Fig. 3 (c).

As for the evenmatched welded joints, the fatigue failure point often originates from W.T. and propagates into the load-carrying plate for the cases of the large penetration length ratios (p/t = 0.7 and 0.5) by the observations from Fig. 3(d) and (e). The fatigue crack initiation points transit from the weld toe to the weld root as the penetration length decreases. Based on the comparisons of fatigue crack points between undermatched welds and evenmatched welds, it is evident that the crack initiation and propagation phases are strongly affected by weld material mechanical strength and local weld geometries. The potential failure modes from the experimental observation are presented in Fig. 3(g). It should be noted that the fatigue crack initiates and propagates from the weld toe and weld root simultaneously for few cases, which is depicted as mode 3 in Fig (g). Thus, it will offer an effective strategy to optimize the fatigue load-carrying capacity considering the effects of local geometries and mechanical mismatch.

3.2. Material cyclic properties

Finite Element (F.E.) simulations of the LCWJ fatigue tests were conducted in Abaqus 6.18, and a nonlinear kinematic Lemaitre-Chaboche material model was offered to simulate the local cyclic mechanical characteristics. Herein, the isotropic and nonlinear kinematic parts of a cyclic hardening model are employed to describe the translation of the yield surface in the stress space by the back stress tensor $\boldsymbol{\alpha}$. The function of the yield surface can be expressed as:

$$f(\sigma - \alpha) = \sigma^0 \tag{1}$$

Table 1
Nominal chemical composition of the BM and weldments [27].

Steel	C(%)	Si(%)	Mn(%)	Cr(%)	Mo(%)	Ni(%)	Cu(%)	V(%)	S(%)	P(%)
10CrNi3MoV	0.09	0.29	0.48	0.94	0.4	2.88	–	0.06	0.005	0.011
U-Welds	0.027	0.243	1.3	0.051	–	1.09	0.033	–	0.0073	0.011

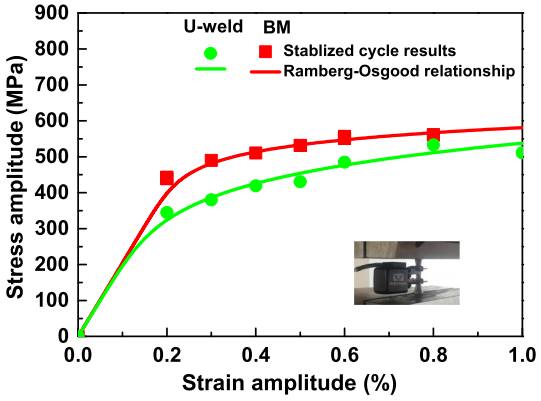

Fig. 1. The cyclic stress–strain curves by R-O relationship equation for base metal and undermatched weldments.

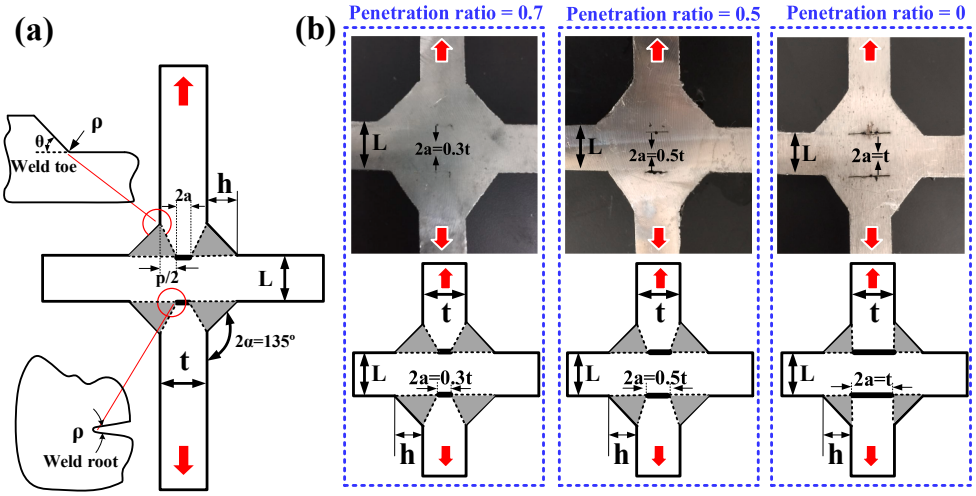

Fig. 2. Geometrical scheme of LCWJs for fatigue tests, (a) geometry details; (b) LCWJs with different penetration ratios [28].

where **σ** denotes the stress tensor, σ^0 is the radius of the yield surface and $f(\sigma\text{-}\alpha)$ is expressed by the following equation:

$$f(\sigma-\alpha)=\sqrt{\frac{3}{2}(S-\alpha^{dev}):(S-\alpha^{dev})} \tag{2}$$

Here α^{dev} is the deviatoric part of the back-stress tensor, and S represents the deviatoric stress tensor.

On the other hand, the kinematic hardening components can be defined by combining a purely kinematic term and a relaxation term, which is shown in the following equation:

$$\alpha=\sum_{i}^{M}\left[C_i\frac{1}{\sigma^0}(\sigma-\alpha)^{\varepsilon^p}-\gamma_i\alpha^{\varepsilon^p}\right] \tag{3}$$

where the C_i and γ_i are the material constants obtained from the cyclic experimental data, C_i strands for the initial kinematic hardening modulus, and γ_i determines the variation rate of kinematic hardening modulus with the increasing plastic deformation. Notably, the determination of C_i and γ_i is made by a multi-linearization fitting of the plastic part data of the material stabilized cyclic curve. *M* stands for the number of couples in the stabilized stress–strain curve, taken as 5 in our study. ε^p represents the equivalent plastic strain rate. The deviatoric term α expresses the deviatoric part depending on the material hardening behavior. With increasing cumulative plastic strain ε^p, the yield surface's size evolves, representing the isotropic hardening property. The isotropic hardening components can be defined by ε^p as:

$$\sigma_0=\sigma|0+Q_{\inf}(1-\exp(-b\cdot\varepsilon^p)) \tag{4}$$

where $\sigma|0$ is the yield stress at the zero-plastic strain. $Q_{\inf}$ denotes the limited value of the yield surface at a significant cumulative

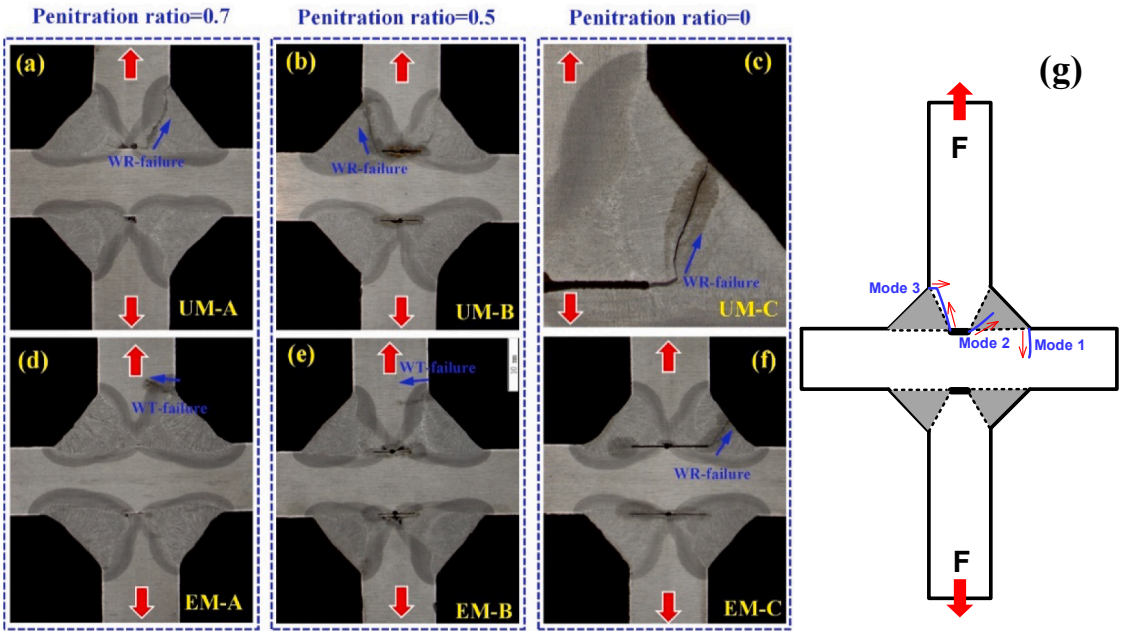

Fig. 3. Crack initiation and propagation locus in the LCF test for different configurations of LCWJ. (a) P ratio = 0.7 for undermatched welds; (b) P ratio = 0.5 for undermatched welds; (c) P ratio = 0 for undermatched welds; (d) P ratio = 0.7 for evenmatched welds; (e) P ratio = 0.5 for evenmatched welds; (f) P ratio = 0 for evenmatched welds; (g) the failure modes of LCWJ [28].

plastic strain, and b is the rate at which the size of the yield surface changes as plastic straining evolution. These material parameters can describe the non-uniformity of the isotropic hardening through-loading cycles of the material. The Bauschinger effect, which is demonstrated with the transition of yield surface, can be expressed by the back stress tensor under cyclic loading.

In order to determine the parameters of the Lemaitre-Chaboche model, the half-cycle stabilized stress–strain curve is used to define by the power-law and five back stresses are determined to approximate the curvature without saturation up to high strain values. The material proprieties from the small-scale bars cyclic tests can further be used to model and analyze the fatigue responses of welded joints. The Chaboche nonlinear kinematic hardening model parameters of base metal and weldments are summarized in [29].

The cyclic plasticity procedure will analyze the case presented in Section 2. The computed notch responses will be compared with a bulk of elastic–plastic numerical analyses by LCWJ FE models. Since the effect of hardening behavior on local notch fatigue indicator, the kinematic hardening material model based on Chaboche cyclic plasticity model was adopted to examine the local cyclic mechanical behaviors in ABAQUS.

3.3. The LCF and HCF tests data

The results of the LCF and HCF test data under different nominal stress and strain ranges are summarized in the S-N plots in Fig. 4,

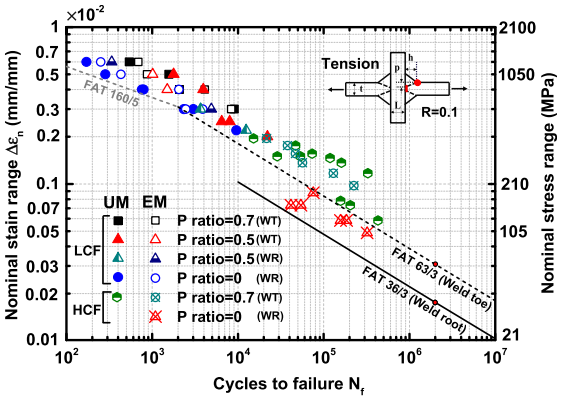

Fig. 4. The LCF and HCF test data under different nominal stress and strain ranges considering the material mismatch ratio and penetration length [28].

which shows the fatigue life as a function of the maximum nominal loading considering the material mismatch ratio, penetration length ratio, failure patterns, and cyclic loading modes. The related reference assessment lines in the HCF regime are added to this figure. The related details about the fatigue test and data illustration are provided in Ref. [28]. Note that an increase of the slope from 3 to 5 for the low cycle fatigue assessment is achieved in this figure. It shows that the FAT160 combined with slope five can satisfy the LCF fatigue test data. The corresponding bound (FAT160/5) could evaluate low cycle S-N curves as the design reference lines, giving safety stock. Regardless, the LCF and HCF test data of LCWJ considering the material yield strength and geometric configurations can provide available references for establishing the suitable design S-N curve of this type of joint.

4. Results of effective notch energy in LCWJs

4.1. Numerical modeling of LCWJs

The finite element model developed to evaluate the evolution of effective notch energy in LCWJs in the elastic–plastic regimes is exhibited in Fig. 5. It was created in a parametric framework, with 8-node hexahedral elements, assuming a homogeneous, linear-elastic, and isotropic material. A refined mesh around the W.T. and W.R. was introduced to describe better the variations of notch stress, strain, and energy. For the remote regions of the LCWJ model, the coarser mesh was adopted, presented in Fig. 5.

4.2. Numerical calculation results of the effective notch strain

The effective notch strain and stress distribution under different loading conditions is the basis for calculating effective notch energy results. The effective notch strain values are often used to assess the local fatigue characteristic indicator in the LCF regime. This section employs the effective notch strain to investigate the fatigue crack initiation relationship in LCWJs. Fig. 6 shows the strain distribution of weld root and weld toe considering penetration ratio effect under cyclic loading conditions for the evenmatched welded joints by the effective notch method. According to the definition of failure modes, the potential fatigue initiation point can be reflected by the maximum strain or energy value. Thus, the fatigue failure point in LCWJ is located at the weld root for the penetration length ratio (p/t = 0.67). With the increases of the penetration length, the fatigue initiation points are transited from the W.R. to W.T. since averaged load carrying strength near these potential failure locations changes, which is presented in Fig. 6(a). When the ratio between weld length and plate thickness was fixed as 1, the strain and stress results were calculated by elastic–plastic mechanical theory. Furthermore, the strain distributions of W.R. and W.T. under different weld lengths are presented in Fig. 6(b). As plotted in Fig. 6(b), the location of maximum strain value transits from W.R. to W.T. as the weld length increases. The smaller weldment is prone to reduce the load-carrying capability for the LCWJs. Similarly, the variation of fatigue failure location in LCWJ occurs under different mismatch ratios, shown in Fig. 6(c). As plotted in the figure, the fatigue crack point initiates at W.T. for overmatched and evenmatched welded joints. With the decreases of the mismatch ratio, the crack initiation point transits to the W.R. for undermatched welded joints due to the increases of local mechanical strength.

4.3. Analytical models of effective notch energy

Our study uses the characteristic energy indicator to assess fatigue behaviors considering the combined effect of local notch stress and strain variations for LCWJs based on the effective notch concept. To illustrate the effects of geometries and material strength mismatch on local mechanical responses, a new notch fatigue characteristic indicator according to the fictitious rounding radius concept was proposed to investigate the LCF and HCF life of LCWJs. The calculations of the notch energy magnitudes can be divided into two phases, including the elastic and plastic mechanical stages. In the elastic phase, the effective notch energy concentration factor K_w^e can be calculated by the stress concentration factor. In contrast, the effective notch energy values in the plastic stage can be deduced by the plastic energy concentration factorK_w^p, which is given in Eq. (1). The formula about effective notch energy value was expressed as following equations [28].

$$\Delta W_{eff}^{root} \ or \ \Delta W_{eff}^{toe} = K_W^N \cdot \Delta W_{nom} = K_W^N \cdot \Delta\sigma_n \cdot \Delta\varepsilon_n = K_W^p \cdot K_W^e \cdot \Delta\sigma_n \cdot \Delta\varepsilon_n \tag{5}$$

where K_w^e is given by:

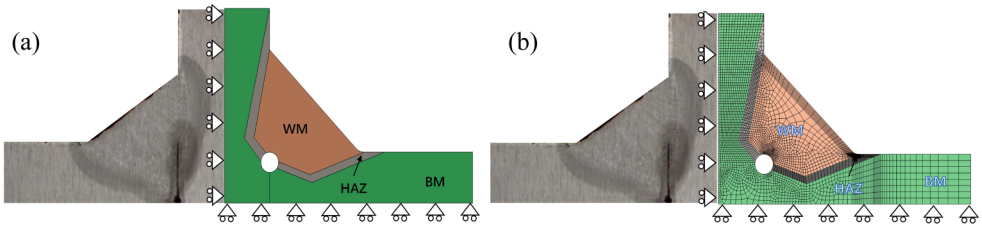

Fig. 5. F.E. models of fatigue characteristic parameters by effective notch method. (a) geometrical model; (b) mesh model.

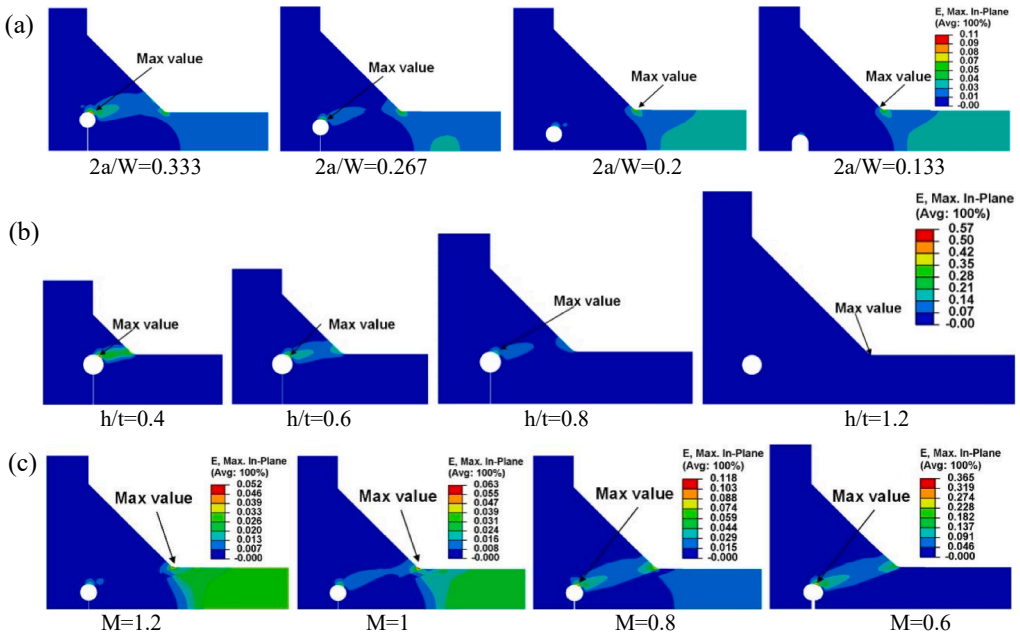

Fig. 6. Strain distribution of LCWJ WR and W.T. under different factors. (a) penetration ratio effect; (b) weld length effect; (c) mismatched ratio effect.

$$K_w^e = \frac{\Delta\sigma_{ij}^e \Delta\varepsilon_{ij}^e}{\Delta\sigma_n \Delta\varepsilon_n} \tag{6}$$

being $\Delta\sigma_{ij}^e$ and $\Delta\varepsilon_{ij}^e$ represent the linear-elastic cyclic stress and strain range at W.T. and W.R. in LCWJ, respectively. $\Delta\sigma_n$ and $\Delta\varepsilon_n$ stand for the nominal stress and strain. The notch energy concentration scheme at W.T. and W.R. of LCWJ is shown according to the fictitious notch rounding concept in Fig. 7.

The notch energy concentration factor K_W^p during the plastic deformation stage was proposed in Ref., which is presented as follows:

$$K_W^P = \left\{ 1 - (1-F)\left(1 - \exp\left(\frac{1}{K_W^e} - \frac{\Delta\sigma_n \cdot \Delta\varepsilon_n}{W_y}\right)\right)^E \right\} \; for \; \Delta\sigma_n \cdot \Delta\varepsilon_n \geqslant W_y / K_N^e \tag{7}$$

where the E and F strands for the characteristic equations related to the material properties and geometries, which are performed as the Eq. (12) and Eq. (13). W_y represents the referenced characteristic energy parameter related to the material yield strength. In the equation, $\Delta\sigma_n$ and $\Delta\varepsilon_n$ are the nominal stress and nominal strain, respectively. The transition phase of the K_W^p is the function of normalized nominal energy indicator ($\Delta\sigma_n\Delta\varepsilon_n/W_y$).

In elastic mechanics regime, the corresponding equations of effective notch energy values at W.T. and W.R. were expressed with the combination of the established geometry characteristic analytical solutions under tension loading in [30], presented as follows:

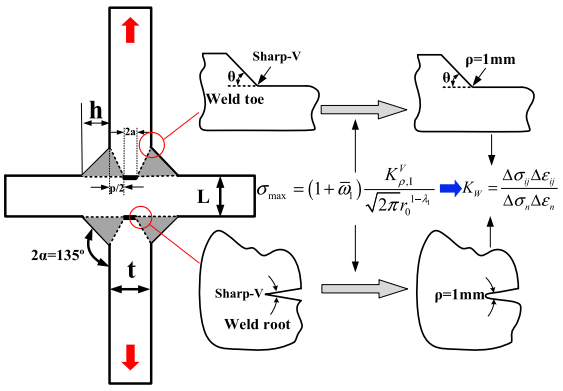

Fig. 7. Illustration of Notch energy concentration factor at WT and WR in LCWJ by fictitious notch rounding concept [28].

$$W.R.: K_{root}^{E} = \left(\frac{\sigma_{\max}}{\sigma_n}\right)^2 = \left(\frac{(1+\overline{\omega}_1)K_1^{root}}{\sigma_n \cdot \sqrt{2\pi}\, r_0^{1-\lambda_1}}\right)^2 = \left(\frac{(1+\overline{\omega}_1)}{\sqrt{2\pi}\, r_0^{1-\lambda_1}} \cdot \frac{k_1^{root}}{\sqrt{e_1}} t^{1-\lambda_1}\right)^2 \tag{8}$$

$$W.T.K_{toe}^{E} = \left(\frac{\sigma_{\max}}{\sigma_n}\right)^2 = \left(\frac{(1+\overline{\omega}_1)K_1^{toe}}{\sigma_n \cdot \sqrt{2\pi}\, r_0^{1-\lambda_1}}\right)^2 = \left(\frac{(1+\overline{\omega}_1)}{\sqrt{2\pi}\, r_0^{1-\lambda_1}} \cdot \frac{k_1^{toe}}{\sqrt{e_1}} t^{1-\lambda_1}\right)^2 \tag{9}$$

$$Where: k_1^{root} = 0.2553 - 7.732 \cdot e^{-1.414(h/t)} + 9.287 \cdot e^{-1.414(h/t)-0.3516(p/t)} \tag{10}$$

$$k_1^{toe} = 1.204 - 1.284 \cdot e^{-3.691(ht)} + 6.8 \cdot e^{-3.177(h/t)-4.707(p/t)} \tag{11}$$

In the Eq. (8), the parameters in the equations of W.T. and W.R. are presented in Table 2. The above equations can estimate the effective notch energy concentration factors in the elastic mechanical regime. Regarding to the plastic mechanic's regime, the related analytical solutions of E and F in Eq. (7) were given in [28], as follows:

$$W.R.: F = 0.9981 \cdot M^{-6.32} \cdot \left(\frac{h}{t}\right)^{-44.968\cdot(1-p/t)+3.8} \cdot \left(-6.09 \cdot \left(1-\frac{p}{t}\right)^{-0.0265} + 6.646\right) \tag{12}$$

$$W.R.: E = M^{0.222} \cdot \left(\frac{h}{t}\right)^{-11.07\cdot(1-p/t)+1.858} \cdot \left(4.99 \cdot \left(1-\frac{p}{t}\right)^{2.387} + 0.301\right) \tag{13}$$

The expression of E and F for weld toe were shown as follows:

$$W.T: F = 1.341 \cdot M^{-11.65\cdot(1-p/t)+0.2026} \cdot \left(\frac{h}{t}\right)^{-33.07\cdot(1-p/t)+2.07} \cdot \left(1.133 \cdot \left(1-\frac{p}{t}\right)^{-0.02017} - 0.8373\right) \tag{14}$$

$$W.T: E = M^{6.929\cdot(1-p/t)-1.522} \cdot \left(\frac{h}{t}\right)^{-10.16\cdot(1-p/t)+2.3} \cdot \left(1.878 \cdot \left(1-\frac{p}{t}\right)^{0.073} - 1.091\right) \tag{15}$$

where the M stands for the mismatch ratio. h/t and p/t represent the ratio of weld length and penetration against the main plate thickness. Combining these equations with those for the elastic regime, the energy concentration factor could be calculated.

4.4. The analytical model results of effective notch energy

4.4.1. Results of plastic notch energy concentration factors

The predicted Plastic Notch Energy Concentration Factors (PNECFs) of W.T. and W.R. with the increasing local plastic deformation degree are calculated by the above proposed analytical solutions, shown as contour plots in Figs. 8-10. The analytical solutions in these figures were presented with the variation of specific weld length h/t, penetration length p/t, and mismatch ratio M, respectively.

The corresponding plastic notch energy concentration factors (PNECFs) at W.T. and W.R. were merged based on effective notch strain and stress magnitudes considering the geometrical and mismatch effect under different penetration lengths, presented in Fig. 8. As shown in Fig. 8, the PNECFs decrease with increases of nominal cyclic loading in the plastic deformation regime for W.R. and W.T. locations. These results at the W.R. point do some variations with penetration length under h/t = 1 in Fig. 8(a), while the results of W.T. mostly keep consistent with the variations of penetration length in Fig. 8(b). It illustrates that the influence of penetration length on PNECF vibration is insignificant for W.T. For more clarity of the weld length on PNECF, Fig. 9 gives the 3D contours for the relationships among PNECF, plastic energy, and weld length. The PNECFs varies significantly with the decreases of weld length under specific penetration ratio (p/t = 0.67) for W.R. and W.T. Notably, according to the discrepancy of PNECFs in Fig. 9(a) and (b), the weld length has a more significant impact on the PNECF of W.R. than the W.T. The variations of PNECFs with mismatch ratios under the penetration ratio (p/t = 0.67) are shown in Fig. 10. A similar tendency can be observed for PNECF magnitudes compared with the results of the weld length effect in Fig. 10. Overall, it demonstrates that weld geometries and material properties greatly influence the PNECFs of failure locations in LCWJ. In addition, it can be seen from the PNECFs under small mismatch ratios can induce tremendous differences in the results of W.R. and W.T.

4.4.2. Comparison of PNECFs between FEA and analytical results

To verify analytical and FEA results of PNECFs under various local geometries and mismatch ratios, three weld length ratios and four mismatch ratios under fixed penetration ratio (p/t = 0.733) have been studied. The weld length ratios are 0.6, 0.8, and 1.2.

Table 2
Geometrical characteristic parameters for weld root and weld toe.

Locations	e_1	λ_1	$\widetilde{w}_1$	s	r_0
Weld root (0°)	0.133	0.5	1	2	1
Weld toe (135°)	0.118	0.674	0.432	4.48	0.869

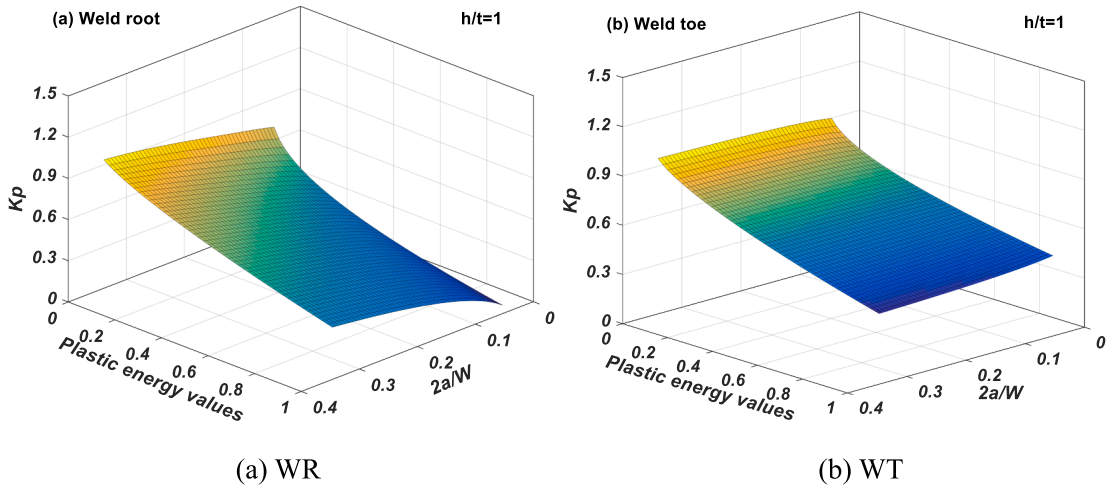

Fig. 8. PNECF distribution at W.R. and W.T. in evenmatched welded joints for different penetration ratios in the case of fixed weld length (h/t = 1).

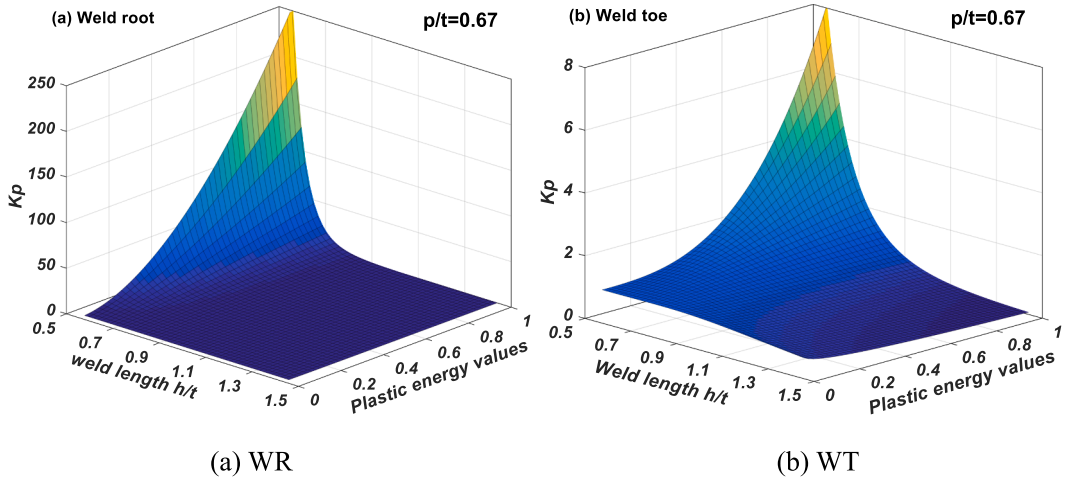

Fig. 9. PNECF distribution at W.R. and W.T. in evenmatched welded joints for different weld length in the case of fixed penetration length (p/t = 0.67).

Meanwhile, the mismatch ratios of 0.6, 0.8, 1, and 1.2 are set to check the results. Comparing the PNECFs of W.R. location under fixed penetration ratio (p/t = 0.733) in Fig. 11(a) and Fig. 11(b), it is found that the PNECFs are both increasing with the decreases of the mismatch ratio and weld length. Meanwhile, good agreements between the F.E. results and the corresponding analytical solutions can be observed. Similarly, the influence of mismatch ratio and weldment geometries on PNECFs is presented in Fig. 11(c) and (d).

4.4.3. Application of the analytical model

To illustrate the variations of notch energy concentration degree under large nominal strain amplitudes, the final notch energy concentration factors (NECFs) were plotted according to the semi-empirical analytical solutions proposed in the above section. We further examine the influence of penetration lengths, weld length, and mismatched ratios on the final Notch Energy Concentration Factor (NECF) by 3D contours, as shown in Fig. 12. For the fixed mismatch ratio M = 1.2, 1, 0.8, 0.6, we see that the NECFs at W.R. and W.T. increase with the decreases of penetration length ratio. A higher penetration length ratio results in an increase of NECF for evenmatched weldment (M = 1.2) at W.R. (Fig. 12(a)) and W.T. (Fig. 12(b)). Under the same configuration of penetration and weld length ratio, a lower mismatch ratio leads to an increase of the magnitudes of NECF at W.R. and W.T. by the comparison of z axial scale among Fig. 12(a), (c), and (e). The same behavior is observed in terms of the effect of weld length ratio on the NECF distribution for the exact failure location, which is presented by the comparison among Fig. 12(b), (d), and (f). Note that the discrepancy exists between the W.T. and W.R. for the same welded joint, judging the fatigue failure initiation. Thus, the proposed analytical solutions can determine the transition relationships of the W.R. and W.T. failures due to the variations of geometries and yield strength in LCWJs.

The quantified transition relationships of the W.R. and W.T. failures under different geometries. The yield strength configurations in LCWJs were explored, as shown in Fig. 13. Regarding the evenmatched CLWJs with fixed penetration length (p/t = 0.67) in Fig. 13

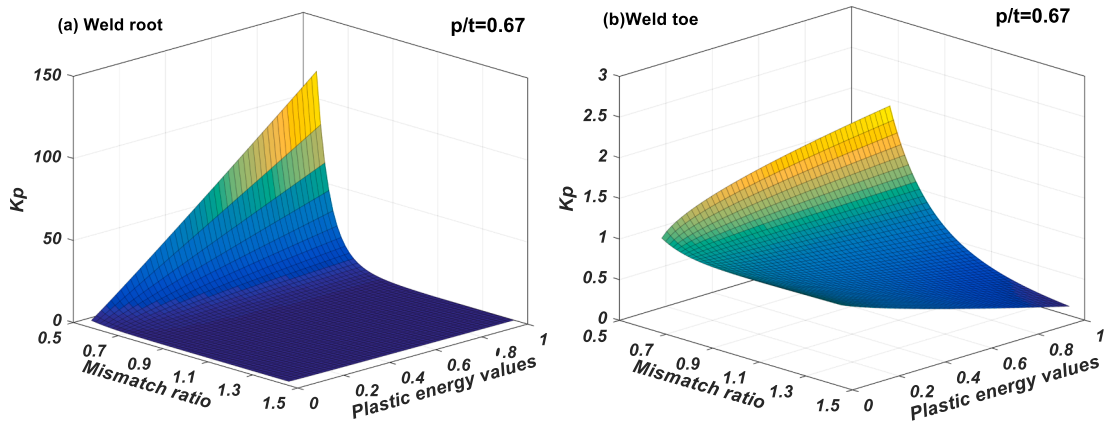

(a) WR (b) WT

Fig. 10. PNECF distribution of W.R. and W.T. for different mismatch ratios in the case of fixed penetration length (p/t = 0.67) and weld length (h/t = 1).

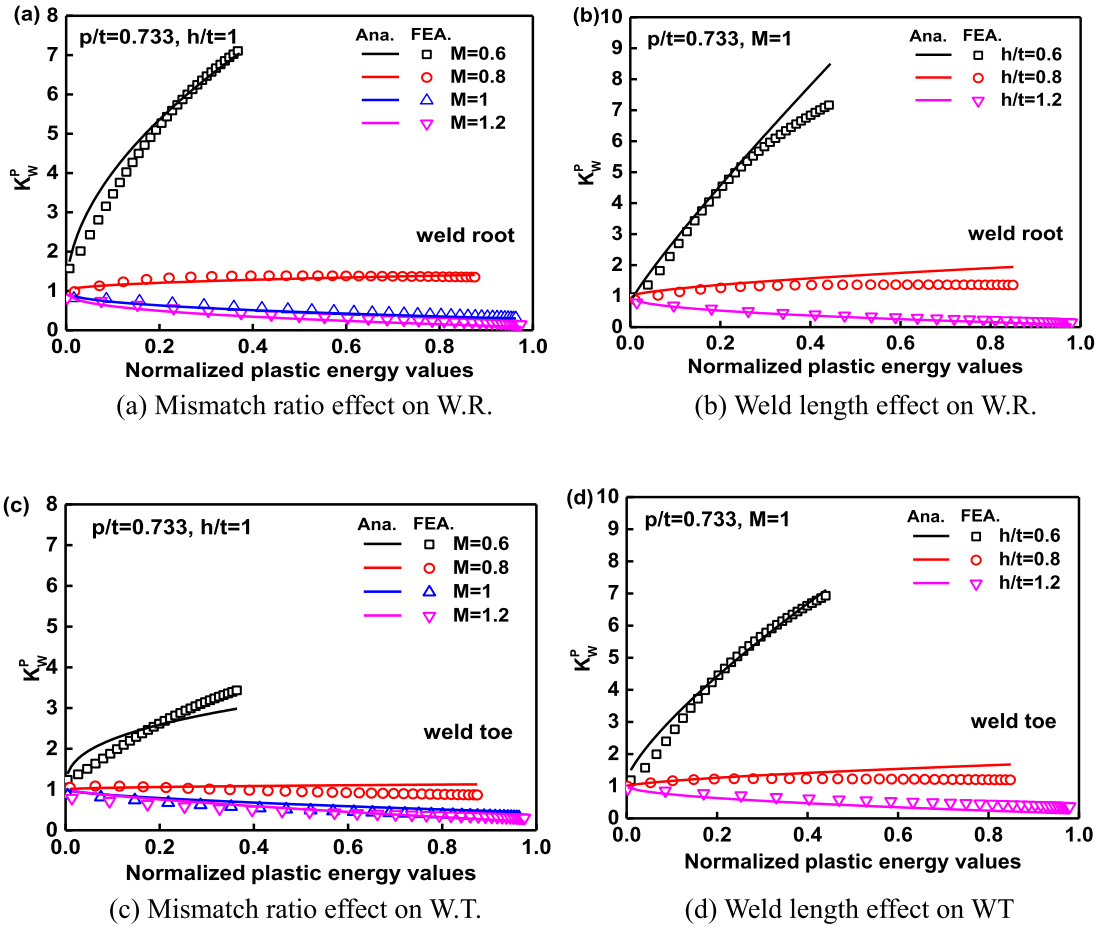

(a) Mismatch ratio effect on W.R. (b) Weld length effect on W.R.

(c) Mismatch ratio effect on W.T. (d) Weld length effect on WT

Fig. 11. Analytical and simulation results comparisons of PNECFs under different geometric and mismatch ratios for the fixed penetration ratio (p/t = 0.733).

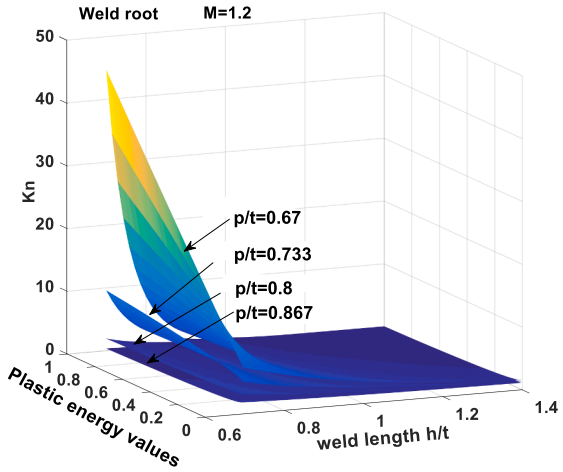

(a) M=1.2 on weld root

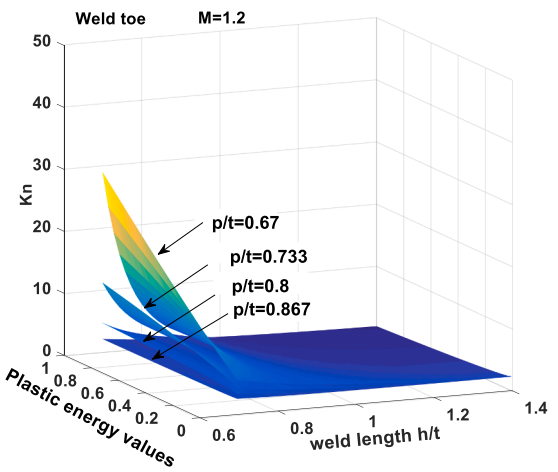

(b) M=1.2 on weld toe

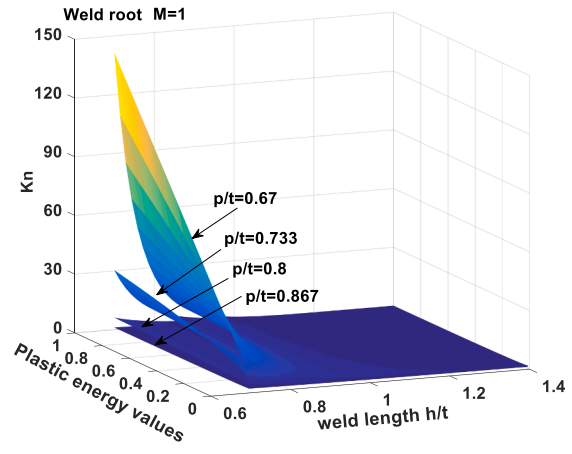

(c) M=1 on weld root

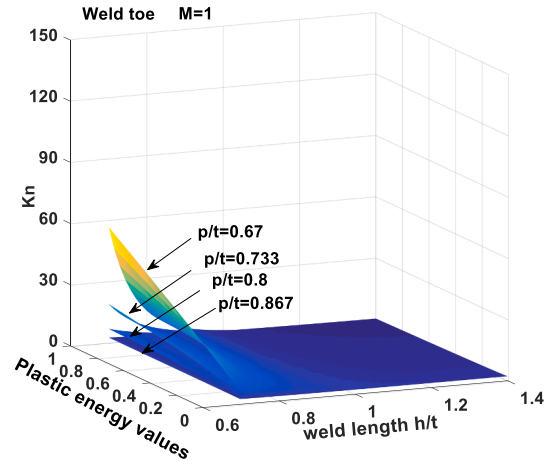

(d) M=1 on weld toe

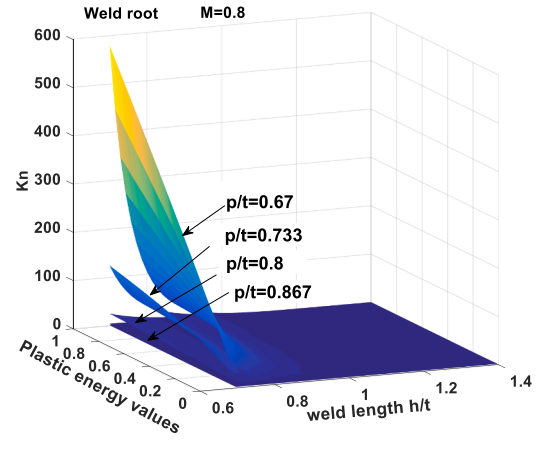

(e) M=0.8 on weld root

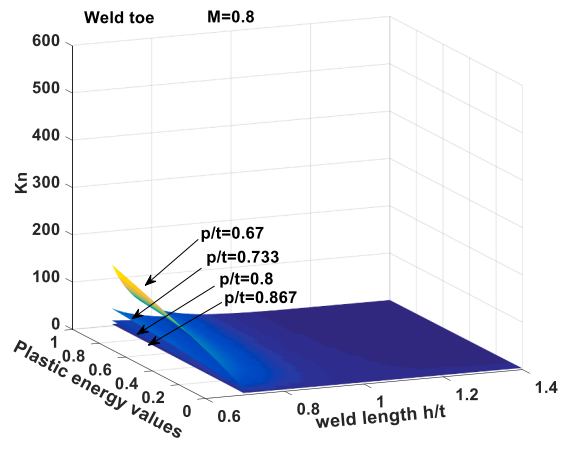

(f) M=0.8 on weld toe

Fig. 12. NECF comparison of different mismatch ratios, penetration ratio, and weld length.

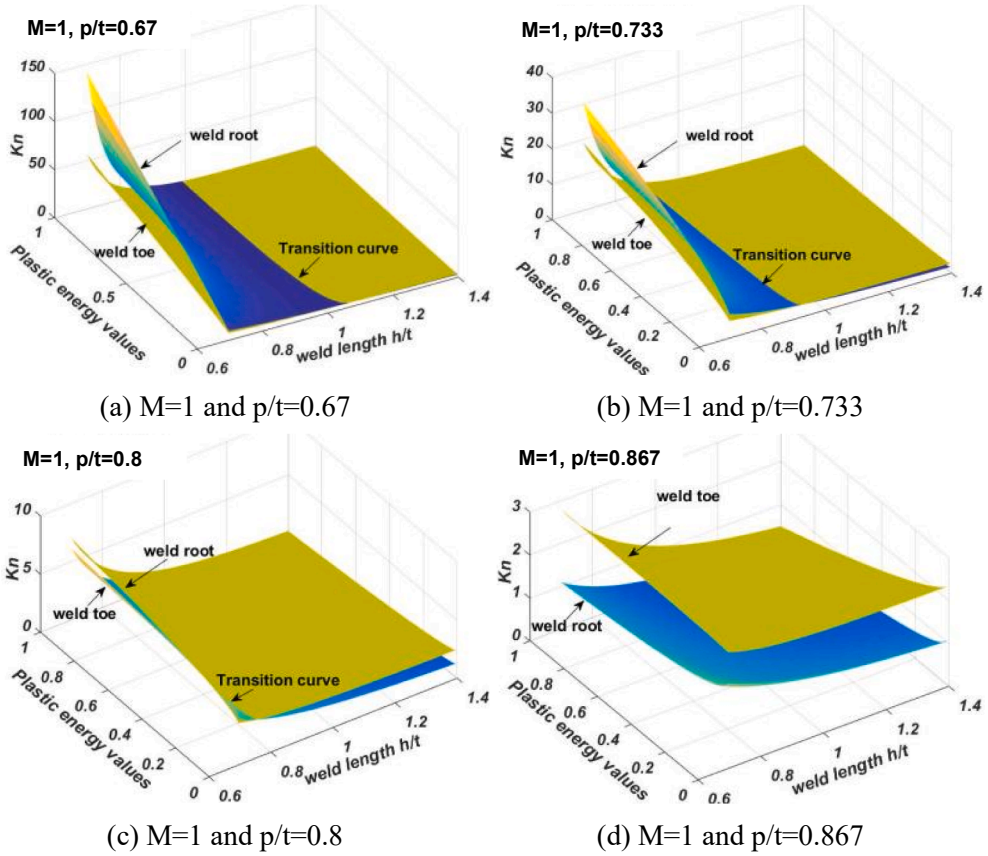

(a) M=1 and p/t=0.67 (b) M=1 and p/t=0.733

(c) M=1 and p/t=0.8 (d) M=1 and p/t=0.867

Fig. 13. Notch energy concentration factor comparison of different mismatch ratios, penetration length ratios, and weld length ratios.

(a), the fatigue failure transition curves between W.T. and W.R. locations for different penetration lengths and weld lengths were determined by intersection line of corresponding 3D contours. The evolution of the transition curves with the increases of penetration length can be examined in Fig. 13(b), (c), and (d). It is seen that the longer penetration length leads to enhancing the load-carrying capacity of the LCWJ, and further makes the W.T. point the potential failure location. Note that the 3D contour of W.T. is entirely higher than that of W.R. location for p/t = 0.867 (Fig. 13(d)) without any intersection point, which implies the final fatigue crack point occurred at the W.T. region. The fatigue failure transition curves with different penetration lengths and weld lengths for evenmatched LCWJs are drawn according to these intersection lines. On the other hand, the different configurations of geometries and mismatch ratios have a similar impact on the transition relationship of fatigue failure locations by deducing intersection lines based on the proposed analytical model. Hence, the transition relationship of fatigue failure location in the LCF regime can be predicted directly from the analytical equations.

According to the previous investigations of the transition curves, the fatigue failure relationship between W.T. and W.R. considering the geometrical variations was characterized by the averaged SED model [31] and Petershagen model [32] based on elastic mechanical theory, which is presented in Fig. 14. As illustrated in Fig. 14(a), the fatigue failure transition curve from the SED model agrees well with the transition line from the Pershagen model [32]. Meanwhile, the transition geometrical relationship data calculated from the proposed notch energy analytical solutions fit the elastic-based transition curves better than the above models. Furthermore, this approach can be extended to examine the transition curve variations considering the mismatch ratio in the LCF regime. The evolution of the fatigue failure transition curves as a function of mismatch ratio in elastic–plastic mechanical regime is presented in Fig. 14(b). It can be seen that the fatigue failure transition curve tends to move to the W.T. direction with the decrease of mismatch ratio. It means that the potential fatigue failure possibility from the W.R. location is more significant than that from the W.T. location. From the observations of the curves, a larger penetration length (p/t) and weld length (h/t) will increase the failure possibility from the W.T. point. However, the reinforced load-carrying capability from the geometrical optimizations seems weaker than the yield strength mismatch ratio due to the geometrical gradient variations from the lines. Therefore, it further illustrates that the mismatch ratio has a more significant influence on the fatigue failure location than the effect of penetration length and weld length.

The fatigue test data and failure relationship of LCWJ considering the W.T. and W.R. locations in both LCF and HCF regimes show in Fig. 15. As presented in Fig. 15(a), the fatigue test data were characterized using the effective notch energy indicator combined with the W.R. and W.T. failure modes considering the mismatch and penetration length ratios [28]. Fig. 15(b) compares failure transition relationship curves considering different mismatch ratios and geometrical factors. The fatigue failure transition curve for evenmatched

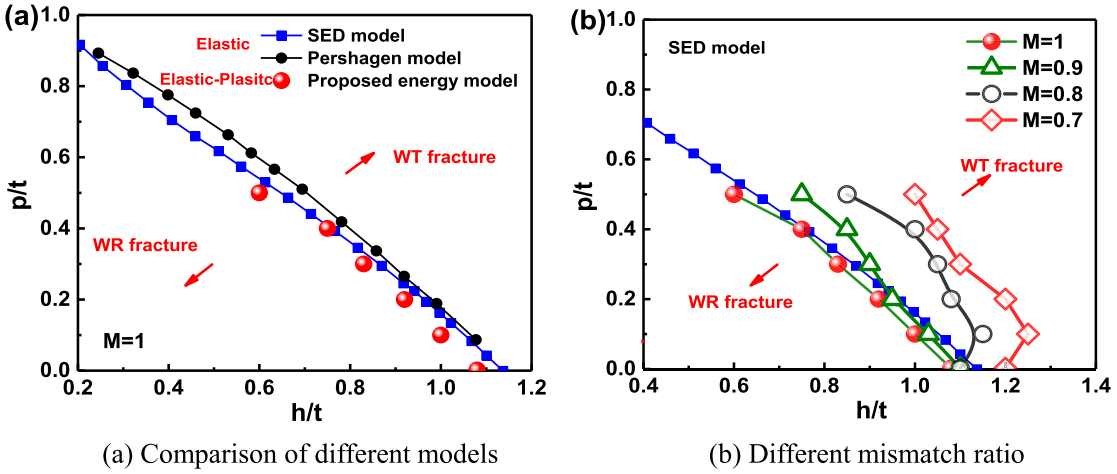

Fig. 14. Comparison of transition curve between weld root and weld toe under different mismatch ratio.

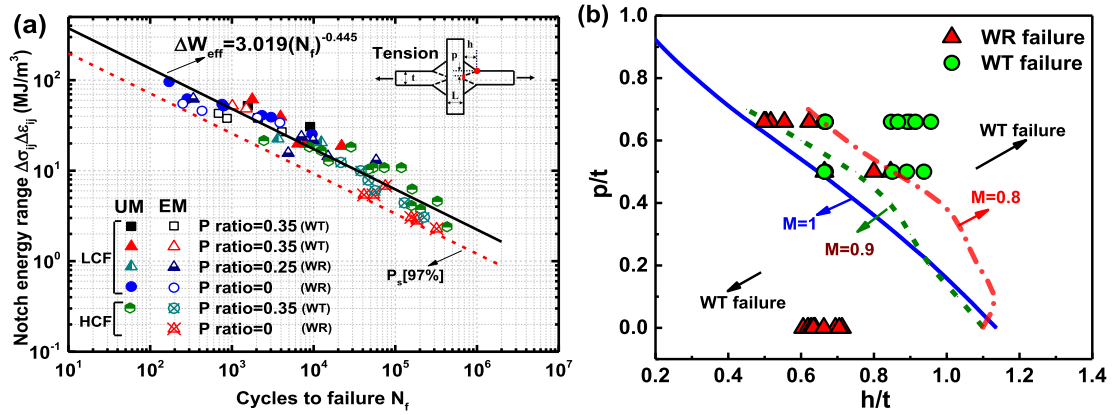

Fig. 15. (a) Fatigue life synthesis of W.T. and W.R. failure in CLWJ based on the notch energy range [28]; (b) Comparison of Failure transition relationship curves considering different mismatch ratios.

welded joints (M = 1) is plotted by the solid blue line. With the decreases of mismatch ratio M, the failure transition boundary between the W.R. and W.T. moves toward the right direction. It indicates that the W.R. failure zone tends to be widened for overmatched cases than for undermatched cases. In Fig. 15(b), the fatigue failure locations according to the experimental data were indicated by the data of solid symbols. The red and green solid symbols represent the W.R. and W.T. failures, respectively. It is evident in Fig. 15 that the fatigue failure transition curve (red dash line) from the analytical model for the specific undermatched ratio (M = 0.8) can differentiate the W.R. and W.T. test data. Hence it validates that the analytical solutions can judge the fatigue crack initiations and assess the transition relationship between W.R. and W.T. failures in LCWJ. It should be noted that there is a possibility from both W.T. and W.R. failure in LCWJ, which induces the difficulty of demining the failure location in the LCF regime.

It is well known that the fatigue life data of welded joints in both HCF and LCF regimes are characterized with high scatter, which can be attributed to many sources. For the LCWJs investigated in the work, the mismatch ratio is the principal factor for the fatigue failure mode transition in the LCF regime, while the geometrical factors become the main effects on the HCF failure behavior, including the penetration weld length. To avoid the stress singularities of notches, an effective notch energy indicator at potential failure points was employed to evaluate the failure modes in LCWJ. The proposed analytical model assessed the above factors quantitatively by effective notch energy indicator based on the elastic–plastic mechanical theory. It is hence reasonable that this model can be used to assess the fatigue failure transition relationships between W.R. and W.T. locations and reduce the scatter by unifying the notch characteristics in LCF and HCF regimes. In our study, the orginal idea for the investigation of fatigue behavior considering the mismatch effect is based on the geometric factor modifications in LCWJ. It is examined to fullfill the engineering needs of determining the geometrical boundary on the fatigue behavior for the production of welded joints. The model will affect the primary joint designs, including the groove, root length, weld length and other weldment details. The equation proposed as a simplified semi-analytical equation for fatigue indicator prediction. Thus, there is no much physical significance.

5. Conclusions

In this work, an analytical model for predicting effective notch energy indicators in LCWJ has been established based on elastic–plastic mechanical theory. It investigates the fatigue failure transition relationship between the W.T. and W.R. locations in the HCF and LCF regimes. The mismatch ratio is incorporated to consider the difference in effective notch energy variations under various loading conditions. The verification analysis and comparative illustration are conducted to verify the validity of the proposed analytical model. The investigations about fatigue failure of LCWJ in this study indicate the following main conclusions:

Three essential parameters, mismatch ratio(M), penetration length ratio (p/t), weld length ratio (h/t), affect the fatigue failure transition relationship between W.T. and W.R. locations. An analytical model is established to characterize effective notch energy in elasto-plastic mechanical regimes, representing the combined effects of these factors.

The effective notch energy approach can be regarded as the fatigue characteristic indicator. The notch energy estimations of LCWJ from the model are in good agreement with the magnitudes by elasto-plastic FEM results. In terms of the Energy-life curves, it can be effective to assess the fatigue strength of LCWJs in HCF and LCF regimes.

According to the comparisons of 3D contours of NECF considering these factors, it is found that the mismatch ratio determines the fatigue failure transition relationships for different geometrical configurations in the LCF regime. The geometrical length could determine the fatigue failure transition relationship of LCWJ in the HCF regime. Finally, the quantitative relationships of fatigue failure transition were determined considering yield strength mismatch and geometrical factors.

Statements of contribution

Wei Song proposed this methodology, did finite element analysis and fatigue tests. Jingzhen Kuang wrote the manuscript. Guangtao Zhou revised the manuscript. Guian Qian and Filippo Berto supervised the findings of this work. All authors discussed the results and contributed to the final manuscript.

Declaration of Competing Interest

The authors declare that they have no known competing financial interests or personal relationships that could have appeared to influence the work reported in this paper.

Acknowledgments

The research project is supported by the National Natural Science Foundation of China (Grant no. 52105403), the Natural Science Foundation of Jiangsu Province (grant no. BK20200174), the Natural Science Foundation of Fujian Province (grant no. 2021J01299), the Postdoctoral Science Foundation of China (2021M702753), the Natural Science Foundation of the Jiangsu Higher Education Institutions (grant no. 20KJB430008), Xuzhou Basic Research Program of Science and Technology (KC21037), and the Qinglan project of Jiangsu province.

References

[1] D. Radaj, C.M. Sonsino, W. Fricke, Fatigue Assessment of Welded Joints by Local Approaches: Second Edition, 2006.
[2] Y. Qin, H. den Besten, S. Palkar, M.L. Kaminski, Mid- and high-cycle fatigue of welded joints in steel marine structures: effective notch stress and total stress concept evaluations, Int. J. Fatigue 142 (2021).
[3] F. Fomin, M. Horstmann, N. Huber, N. Kashaev, Probabilistic fatigue-life assessment model for laser-welded Ti-6Al-4V butt joints in the high-cycle fatigue regime, Int. J. Fatigue 116 (2018) 22–35.
[4] Z. Mikulski, T. Lassen, Fatigue crack initiation and subsequent crack growth in fillet welded steel joints, Int. J. Fatigue 120 (2019) 303–318.
[5] F. Berto, P. Lazzarin, Fatigue strength of structural components under multi-axial loading in terms of local energy density averaged on a control volume, Int. J. Fatigue 33 (2011) 1055–1065.
[6] F. Berto, P. Lazzarin, A review of the volume-based strain energy density approach applied to V-notches and welded structures, Theor. Appl. Fract. Mech. 52 (2009) 183–194.
[7] C.M. Sonsino, Course of SN-curves especially in the high-cycle fatigue regime with regard to component design and safety, Int. J. Fatigue 29 (2007) 2246–2258.
[8] K. Saiprasertkit, T. Hanji, C. Miki, Fatigue strength assessment of load-carrying cruciform joints with material mismatching in low- and high-cycle fatigue regions based on the effective notch concept, Int. J. Fatigue 40 (2012) 120–128.
[9] L. Feng, X. Qian, Size effect and life estimation for welded plate joints under low cycle actions at room and low ambient temperatures, Thin-Walled Struct. 132 (2018) 195–207.
[10] A. Hobbacher, Recommendations for fatigue design of welded joints and components: IIW document IIW-1823-07 ex XIII-2151r4-07/XV-1254r4-07, Recommendations for Fatigue Design of Welded Joints and Components (2008).
[11] I. Lotsberg, G. Sigurdsson, Hot spot stress S-N curve for fatigue analysis of plated structures, J. Offshore Mech. Arct. Eng. 128 (2006) 330–336.
[12] P. Dong, J.K. Hong, The master S-N curve approach to fatigue of piping and vessel welds, Welding in the World 48 (2004) 28–36.
[13] H. Kyuba, P. Dong, Equilibrium-equivalent structural stress approach to fatigue analysis of a rectangular hollow section joint, Int. J. Fatigue 27 (2005) 85–94.
[14] H. Lu, P. Dong, S. Boppudi, Strength analysis of fillet welds under longitudinal and transverse shear conditions, Mar. struct. 43 (2015) 87–106.
[15] G. Alencar, J.K. Hong, A. de Jesus, J.G.S. da Silva, R. Calçada, The Master S-N curve approach for fatigue assessment of welded bridge structural details, Int. J. Fatigue 152 (2021), 106432.
[16] P. Wang, X. Pei, P. Dong, S. Song, Traction structural stress analysis of fatigue behaviors of rib-to-deck joints in orthotropic bridge deck, Int. J. Fatigue 125 (2019) 11–22.
[17] Z. Wei, H. Jin, G. Chen, Traction structural stress analysis of fatigue behaviors of girth butt weld within welded cast steel joints, Int. J. Press. Vessels Pip. 179 (2020) 104027.
[18] S. Xing, P. Dong, A. Threstha, Analysis of fatigue failure mode transition in load-carrying fillet-welded connections, Mar. struct. 46 (2016) 102–126.
[19] S. Xing, P. Dong, Fatigue of titanium weldments: S-N testing and analysis for data transferability among different joint types, Mar. Struct. 53 (2017) 1–19.
[20] S. Xing, P. Dong, P. Wang, A quantitative weld sizing criterion for fatigue design of load-carrying fillet-welded connections, Int. J. Fatigue 101 (2017) 448–458.
[21] S. Xing, P. Dong, An analytical SCF solution method for joint misalignments and application in fatigue test data interpretation, Mar. Struct. 50 (2016) 143–161.

[22] K. Saiprasertkit, T. Hanji, C. Miki, Local strain estimation method for low- and high-cycle fatigue strength evaluation, Int. J. Fatigue 40 (2012) 1–6.
[23] K. Saiprasertkit, E. Sasaki, C. Miki, Fatigue crack initiation point of load carrying cruciform joints in low and high cycle fatigue regions, Int. J. Fatigue 59 (2014) 153–158.
[24] Y. Dong, Y. Garbatov, C. Guedes Soares, Improved effective notch strain approach for fatigue reliability assessment of load-carrying fillet welded cruciform joints in low and high cycle fatigue, Mar. Struct. 75 (2021), 102849.
[25] P. Dong, X. Pei, S. Xing, M.H. Kim, A structural strain method for low-cycle fatigue evaluation of welded components, Int. J. Press. Vessels Pip. 119 (2014) 39–51.
[26] X. Pei, P. Dong, S. Xing, A structural strain parameter for a unified treatment of fatigue behaviors of welded components, Int. J. Fatigue 124 (2019) 444–460.
[27] W. Song, X. Liu, F. Berto, S.M.J. Razavi, Low-cycle fatigue behavior of 10CrNi3MoV high strength steel and its undermatched welds, Materials 11 (5) (2018) 661.
[28] W. Song, X. Liu, G. Zhou, S. Wei, D. Shi, M. He, F. Berto, Notch energy-based low and high cycle fatigue assessment of load-carrying cruciform welded joints considering the strength mismatch, Int. J. Fatigue 151 (2021) 106410.
[29] W. Song, X. Liu, J. Xu, Y. Fan, D. Shi, F. Yang, X. Xia, F. Berto, D. Wan, Low-Cycle Fatigue Life Prediction of 10CrNi3MoV Steel and Undermatched Welds by Damage Mechanics Approach, Front. Mater. 8 (2021).
[30] P. Livieri, P. Lazzarin, Fatigue strength of steel and aluminium welded joints based on generalised stress intensity factors and local strain energy values, Int. J. Fract. 133 (2005) 247–276.
[31] W. Song, X. Liu, F. Berto, P. Wang, H. Fang, Fatigue failure transition analysis in load-carrying cruciform welded joints based on strain energy density approach, Fatigue Fract. Eng. Mater. Struct. 40 (2017) 1164–1177.
[32] D. Radaj, C.M. Sonsino, Fatigue assessment of welded joints by local approaches, England, Cambridge, 2006.